Geophys. J. R. astr. Soc. (1976) **45**, 583–600.

A Geomagnetic Variation Anomaly in the Northern Pyrenees*†

K. Babour and J. Mosnier

Centre de Recherches Géophysiques, Laboratoire de Géomagnétisme. 24, rue Lhomond, 75231 Paris Cedex 05

M. Daignieres and G. Vasseur

Centre Géologique et Géophysique—Université des Sciences et Techniques du Languedoc—34060 Montpellier Cedex

J. L. Le Mouel and J. C. Rossignol

Institut de Physique du Globe—4 place Jussieu—75230 Paris Cedex 05

(Received 1975 December 29; in original form 1975 October 10)

Summary

Sixty stations measuring the time variations of the Earth's magnetic field were operated from 1972 to 1974 in the Northern Pyrenees. Magnetograms show a very large anomaly in the vertical and horizontal variation fields for the period range from a few minutes to a few hours. Owing to the particular measurement and reduction techniques used it was possible to show that, for the above period range, the anomalous field is the product of a function of space by a function of time. This anomaly corresponds to a current concentration the geometry of which is *invariant* with time. Most of the currents associated with the anomaly flow at a depth smaller than 15 km. The orientation of the conductive structure is different from the orientation of superficial structures; this structure could correspond to old sedimentary basins inside the palaeozoic basement or (and) to a hidden accident in the basement as suggested by seismic evidence.

1. Introduction

Time variations of the Earth's magnetic field have been recorded in the eastern part of the Pyrenees during various periods in the years 1972–73–74. This study was at first designed to look for a possible geomagnetic anomaly associated with the North Pyrenean fault (Choukroune, Séguret & Galdeano 1973). About 60 stations were occupied altogether. A very large anomaly of the transient variations of the

* IPGP NS Contribution No. 175.
† CGGM contribution No. 189.

Downloaded from https://academic.oup.com/gji/article/14/583/570157 by U.S. Department of Justice user on 17 August 2022

geomagnetic field was indeed found, although its relation to the North Pyrenean fault is not certain. Owing to the great number of stations operated, it was possible to describe adequately the characteristics of this anomaly.

We will first describe the equipment used and the data processing. Then, we will discuss the main characteristics of the anomaly. Finally, we will briefly review the results of complementary experiments carried out in the same area and the data provided by other branches of the Earth Sciences.

2. Equipment and field experiments

Two kinds of magnetometers were at our disposal: three-component model GV3 Askania variographs (for their characteristics, see for example Schmucker 1970) and more modern suspended-magnet horizontal variometers designed by J. Mosnier (Mosnier 1970; Mosnier & Yvetot 1972).

Five Askania variographs, recording the variations of the three components H, D, Z, of the geomagnetic field were operated together, while six Mosnier horizontal variographs recording the variations of H and D were also operated together. Operational problems prevented the 11 instruments from being operated simultaneously for a long period of time. Each Mosnier station (S_i) was equipped with a telemetric link, transmitting the values $H_i(t)$, $D_i(t)$ recorded at S_i to a central reference station S_0. Thus it was possible to record the various differences $\Delta H_{i0}(t) = H_i(t) - H_0(t)$ and $\Delta D_{i0}(t) = D_i(t) - D_0(t)$ ($i = 1, 2, 3, 4, 5$) in real time. As for the GV3 Askania variographs of lesser sensitivity, they were especially useful because of the $Z(t)$ record they provided.

Location of stations

We had to take into account different requirements to avoid industrial interference, but ensure the electrical power supply and, as far as Mosnier variometers were concerned, the need of a direct line of sight between stations S_i and the central station S_0. With these considerations in mind, we tried to cover the studied area uniformly as is shown in Fig. 1. As a general rule, the stations were distributed along approximately north–south profiles, (geological structures, especially the North Pyrenean fault, having an east–west trend in this region). Four profiles (A'A, B'B, C'C and D'D on Fig. 1) were obtained with the Askania instruments and three ($\alpha'\alpha$, $\beta'\beta$, and $\gamma'\gamma$ on Fig. 1) with the Mosnier variographs. The average distance between two profiles is about 20 km; the average distance between two stations of a given profile is about 15 km.

3. Examples of magnetograms

Fig. 2(a) shows three sets of simultaneous recordings of the components H, D, Z given by the Askania variographs: the recordings of 1974 October 18 (A'A profile), those of 1974 September 25 (B'B profile) and those of 1973 September 2 (C'C profile). One can notice that the variations of the vertical component have opposite signs in the north and south of each profile and become zero near points A'', B'' and C'' along each profile (Fig. 1). At the stations where they reach a maximum, the variations of the Z component may be up to 50 per cent of the simultaneous variations of the horizontal components.

Fig. 2(b) shows recordings $H_0(t)$, $D_0(t)$ of the components H and D obtained on 1973 October 5–6 with the Mosnier variometers at station S_0 (PDN) and the simultaneous recordings of the differences $\Delta H_{i0}(t)$, $\Delta D_{i0}(t)$ ($i = 1, 5$) between the horizontal components measured at the stations S_i of profile $\gamma'\gamma$ and those from station S_0.

Downloaded from https://academic.oup.com/gji/article/1/4/583/570157 by U.S. Department of Justice user on 17 August 2022

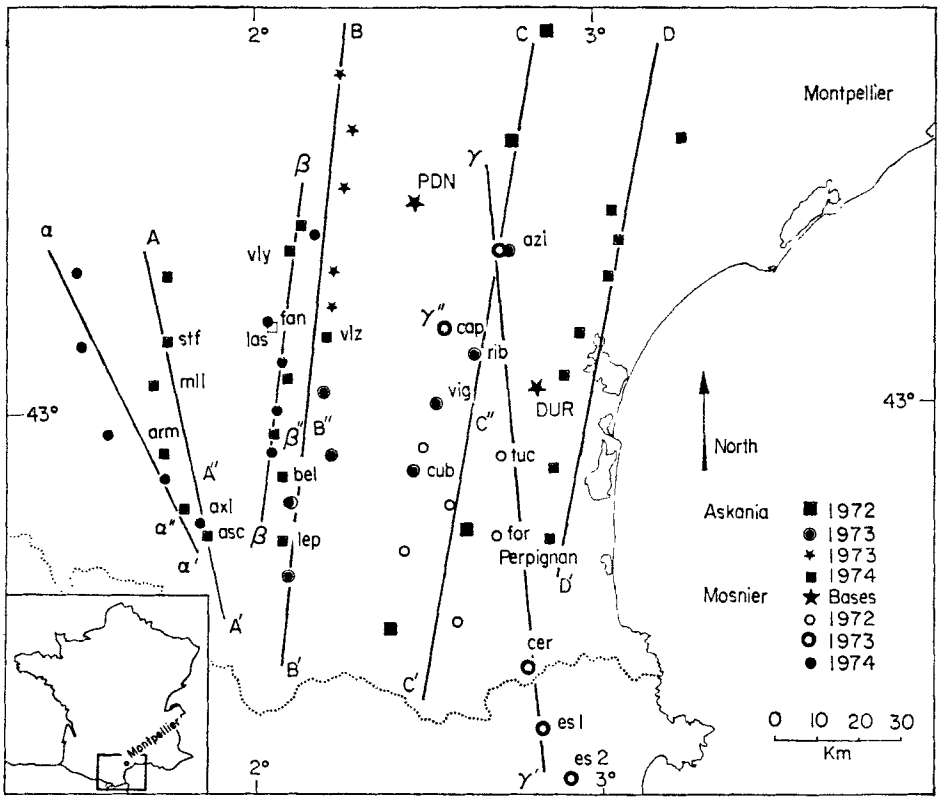

FIG. 1. Location of the stations in the Northern Pyrenees. The different types of variometers and the time of experiment are distinguished with different symbols. Bottom left: situation of the studied area.

(The choice of PDN as a reference station will be discussed later.) It can be seen that the curves representing the differences $\Delta H_{i0}(t)$, $\Delta D_{i0}(t)$ at one station S_i are very similar to those at any other station S_j; however, they are clearly different from the $H_0(t)$ and $D_0(t)$ variations recorded simultaneously. In the station where it is a maximum (CAP on Fig. 2(b)), the amplitude of the variations $\Delta H_{i0}(t)$ is of the same order as that of the simultaneous variations $H_0(t)$ or $D_0(t)$. The similarity of the $\Delta H_{i0}(t)$ and $\Delta D_{i0}(t)$ recordings shown on Fig. 2(b) holds for all the simultaneous recordings of differences made along profiles $\alpha'\alpha$ and $\beta'\beta$. The $\Delta H_{i0}(t)$ differences reach their maximum amplitude near the points α'', β'' and γ'', respectively along profiles $\alpha'\alpha$, $\beta'\beta$, and $\gamma'\gamma$ (Fig. 1).

Fig. 2(c) shows recordings of the differences $\Delta H_{i0}(t)$, $\Delta D_{i0}(t)$ (S_i = FAN, on the $\beta'\beta$ profile, S_0 = PDN) as well as a simultaneous recordings of the vertical component at station PDN. The similarity between these three curves is again striking.

4. Characteristics of the anomaly

Normal and anomalous field

The transient field at observation point P, $\vec{B}(P, t)$, can be decomposed into two terms (Schmucker 1970; Gough 1973): $\vec{B}(P, t) = \vec{B}_n(P, t) + \vec{B}_a(P, t)$ where $\vec{B}_n(P, t)$ is the normal field that would be observed in a layered Earth, while $\vec{B}_a(P, t)$ is the anomalous field created by lateral variations in the distribution of conductivity.

Downloaded from https://academic.oup.com/gji/article/14/583/570157 by U.S. Department of Justice user on 17 August 2022

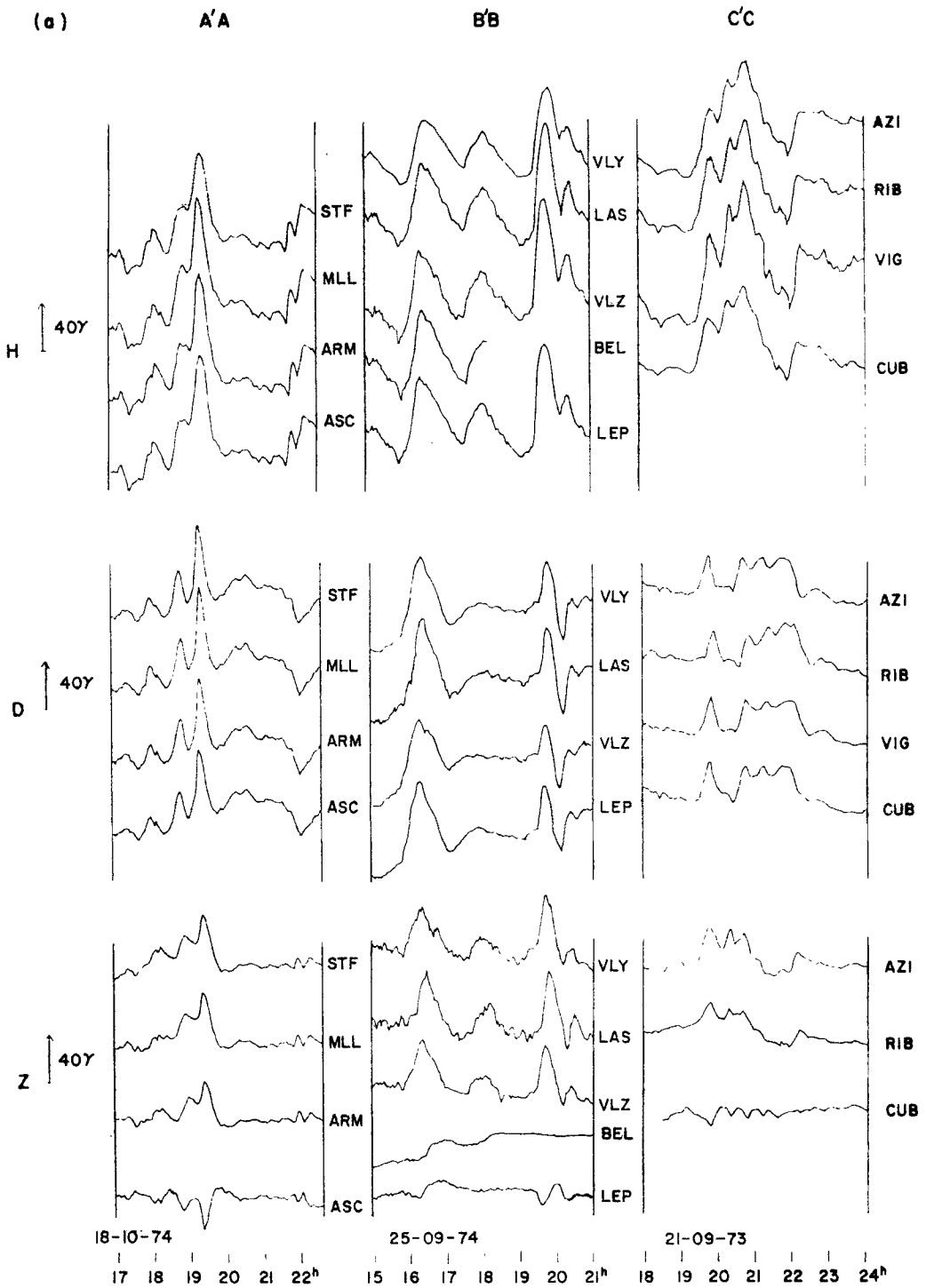

FIG. 2.(a) Magnetograms of 1974 Oct. 18; 1974 Sept. 25; 1973 Sept. 21; respectively along profiles A'A, B'B, C'C of Fig. 1.

Downloaded from https://academic.oup.com/gji/article/1/4/583/570157 by U.S. Department of Justice user on 17 August 2022

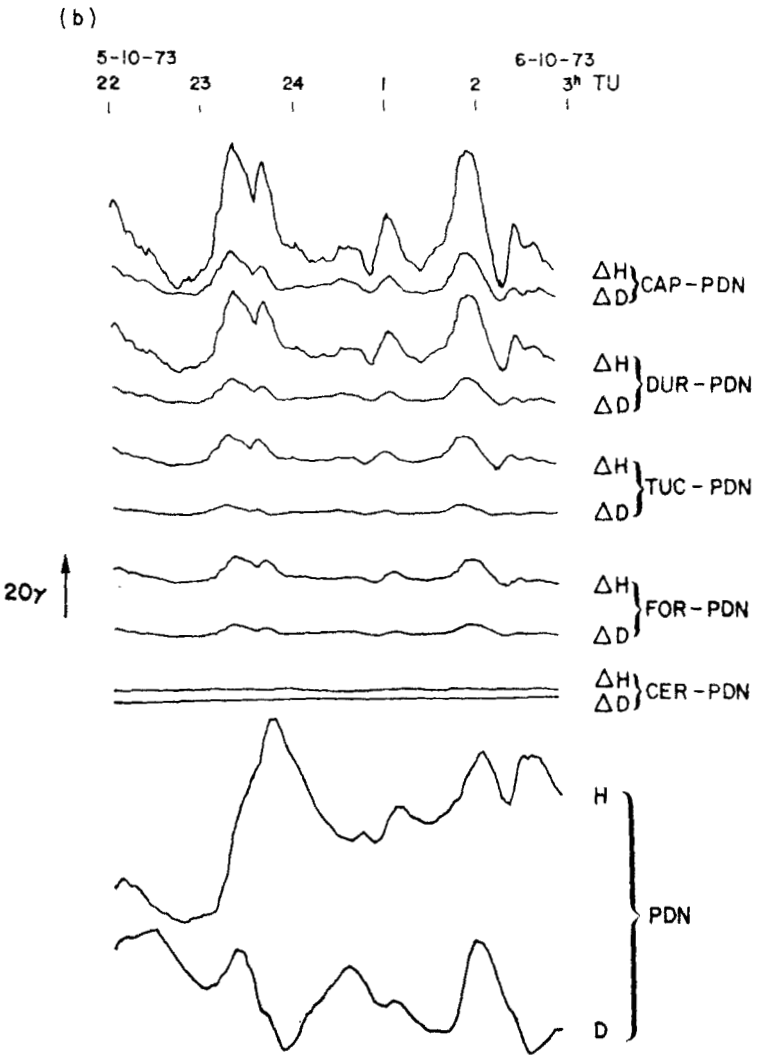

FIG. 2(b) Top: differences $\Delta H_{i0}(t)$, $\Delta D_{i0}(t)$ for the stations S_i of profile $\gamma'\gamma$ of Fig. 1 on 1973 Oct. 5–6. Bottom: simultaneous records of H and D components at the PDN station.

Since the normal field can be considered as uniform in the studied area—whose linear dimensions are about 100 km—the differences $\overrightarrow{\Delta B}$ between station S_i and station S_0 are reduced to the differences $\overrightarrow{\Delta B_a}$. Let us now suppose that the reference station S_0 is a normal one, that is to say that $\vec{B}_a(S_0, t) = 0$. Then $\overrightarrow{\Delta B_{i0}}(t) = \vec{B}_a(S_i, t)$; the observed difference between S_i and S_0 reduces to the anomalous field $\vec{B}_a$ at S_i.

In practice a station will be called normal when it is located in the centre of an area where the differences ΔH and ΔD are systematically small compared with the differences ΔH, ΔD simultaneously observed in the area of the anomaly. Such is the case for the station of Ceret (CER): the differences ΔH and ΔD between Ceret and the three stations labelled ES1, ES2 and LAB on Fig. 1 are systematically less than

Downloaded from https://academic.oup.com/gji/article/1/4/583/570157 by U.S. Department of Justice user on 17 August 2022

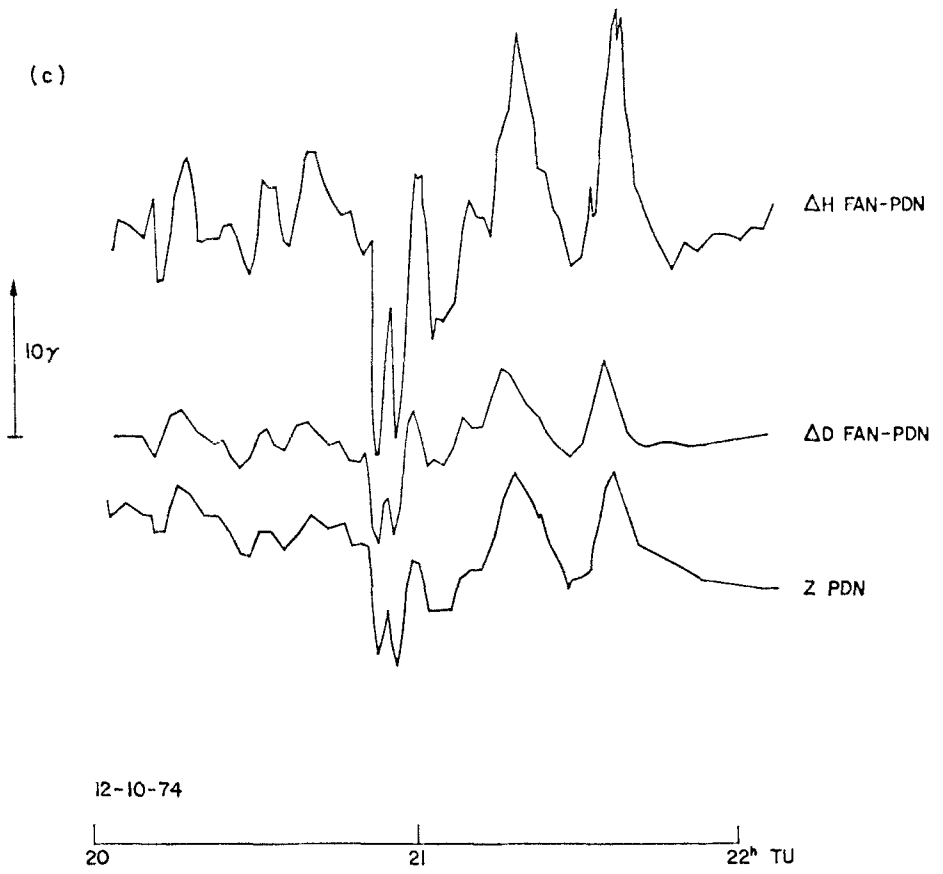

FIG. 2(c) Simultaneous variations of $Z(t)$ at S_0 = PDN and of $\Delta H_{i0}(t)$, $\Delta D_{i0}(t)$ at S_i = FAN on 1974 Oct. 12.

0·2γ for variations of H and D reaching 100γ, and this whatever the type of disturbance be. So the CER station may be considered as normal as far as the studied anomaly, the wavelength of which is typically 100 km (*cf.* Fig. 2), is concerned. As the horizontal differences between the PDN and CER stations are null (Fig. 2(b)), the PDN station may be taken as a reference station S_0 for the horizontal components as well as the CER station, even though it is not normal in the sense defined above (in particular, large vertical variations $Z(t)$ are observed at PDN (*cf.* Fig. 2(c)). For practical reasons (in particular in order to have direct sight between the reference stations S_0 and the satellite stations S_i), PDN was chosen as a reference station for horizontal components in all the present study; all things are as if the CER station had been chosen as the reference.

Horizontal component of the anomalous field

What has been previously observed in the example of Fig. 2(b) holds, as we said, for all the recordings of differences made in the studied region: all the simultaneous curves representing the differences $\Delta H_{i0}(t)$, $\Delta D_{i0}(t)$, $\Delta H_{j0}(t)$, $\Delta D_{j0}(t)$ and, consequently, the differences $\Delta H_{ij}(t)$, $\Delta D_{ij}(t)$ (whatever the couple i, j may be) are rigorously similar to one another in the whole period range from a few minutes to a few hours (the

Downloaded from https://academic.oup.com/gji/article/14/583/570157 by U.S. Department of Justice user on 17 August 2022

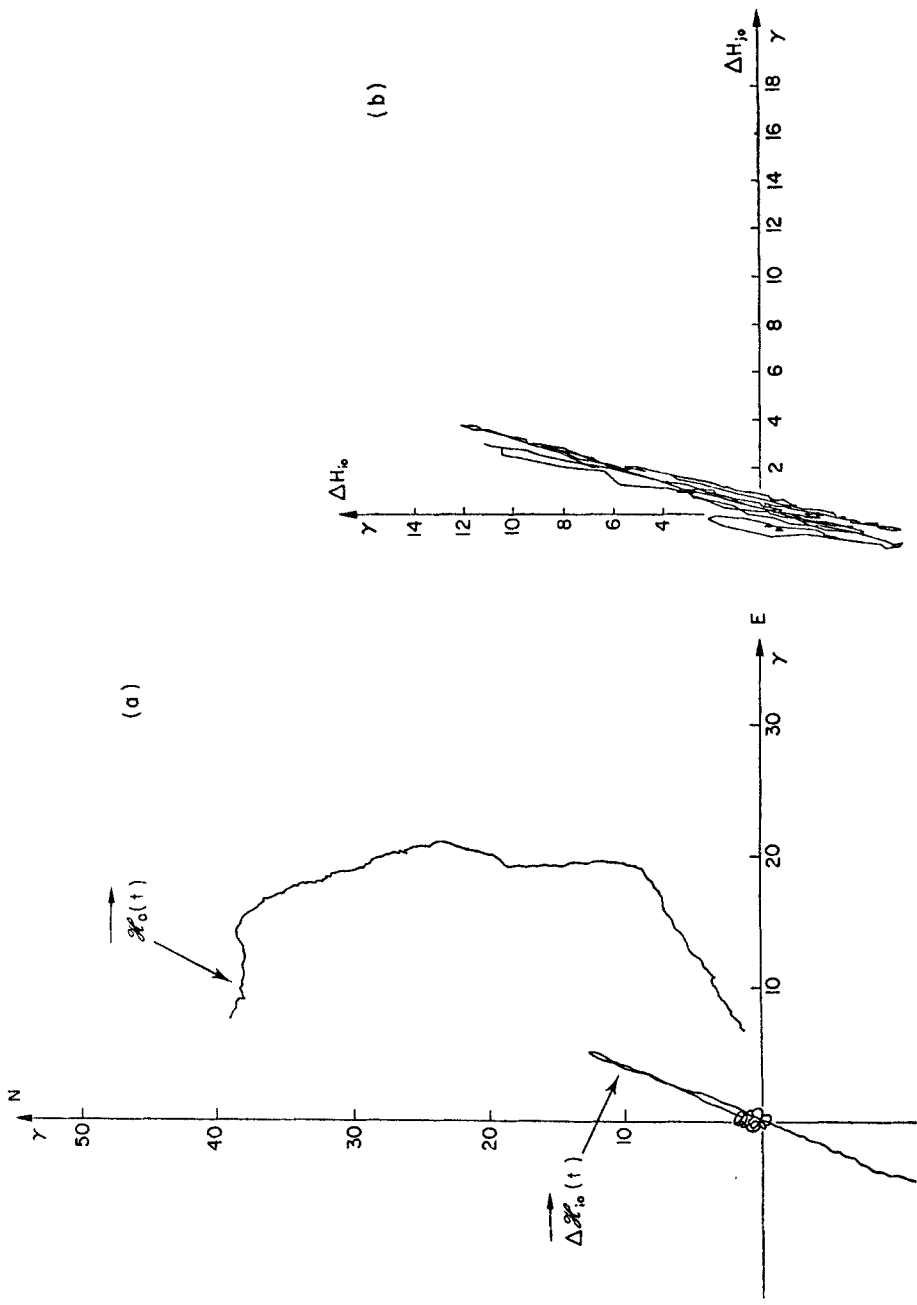

FIG. 3. (a) Hodograph of $\overrightarrow{\Delta\mathscr{H}_{i0}}(t)$ and $\overrightarrow{\mathscr{H}_0}(t)$ on 1974 Oct. 1; S_i = FAN, S_0 = PDN. (b) Hodograph of the vector ($\Delta H_{i0}(t)$, $\Delta H_{j0}(t)$) on 1974 Oct. 17; S_i = DUR; S_j = FAN.

Downloaded from https://academic.oup.com/gji/article/1/4/583/570157 by U.S. Department of Justice user on 17 August 2022

differences ΔH, ΔD have no measurable time variations with periods, or time constants, larger than 4 hr; for periods smaller than a few minutes, the perfect similarity between one station and one other is no more observed; but the amplitude of these short period variations is generally weak). Fig. 3 illustrates the accuracy of the similarity: the plots of the extremities of the horizontal vectors $\overrightarrow{\Delta\mathscr{H}}_{i0}(t) = (\Delta H_{i0}(t), \Delta D_{i0}(t))$ on one hand, and of $(\Delta H_{i0}(t), \Delta H_{j0}(t))$ on the other hand follow straight lines; the small deviation of hodographs from straight lines are due to measurement errors and to the presence of short period pulsations (30–50 s) at the FAN station (these pulsations appear to be drastically attenuated at the PDN station).

In other words, in the periods range from a few minutes to a few hours, the field of the horizontal differences $\overrightarrow{\Delta\mathscr{H}}_{i0}(t)$ has the following properties:

(a) It is strictly linearly polarized at all stations S_i;

(b) the transformation leading from $\overrightarrow{\Delta\mathscr{H}}_{i0}(t)$ observed at S_i to $\overrightarrow{\Delta\mathscr{H}}_{j0}(t)$ observed at S_j is a linear transformation, which depends on the couple (i, j) but is independent of time. These remarkable properties observed at all the stations S_i must be, on account of continuity, valid at any point P of the area concerned. Thus, it can be deduced that the field of horizontal differences $\overrightarrow{\Delta\mathscr{H}}_0(P, t)$ between any point P and the reference station S_0 has the following form:

$$\overrightarrow{\Delta\mathscr{H}}_0(P, t) = \overrightarrow{\Delta h}(P).R(t) \tag{1}$$

Time and space variables are *naturally separated.*

In this formula, $\overrightarrow{\Delta h}(P)$ and $R(t)$ are both defined to within a multiplicative constant, the product of these two terms being the only known quantity. We can, for instance, chose for $R(t)$: $\sqrt{(\Delta H^2{}_{10}(t) + \Delta D^2{}_{10}(t))}$, S_1 being one of the stations S_i, and S_0 being the reference station. Formula (1) means that the field of differences $\overrightarrow{\Delta\mathscr{H}}(P, t)$ has a fixed geometry. If we take the Fourier transform of (1), we see immediately that the geometry of the anomaly does not depend on frequency.

Now, S_0 is supposed to be a normal station (*cf.* discussion above). Then:

$$\overrightarrow{\Delta\mathscr{H}}_0(P, t) = \overrightarrow{\mathscr{H}}_a(P, t)$$

$\overrightarrow{\mathscr{H}}_a(P, t)$ being the horizontal component of the anomalous field $\vec{B}_a(P, t)$. So, this horizontal component may be written in the form:

$$\overrightarrow{\mathscr{H}}_a(P, t) = \vec{h}_a(P).R(t). \tag{2}$$

We are going to see now that the same holds for the three-dimensional anomalous vector field $\vec{B}_a(P, t)$ itself.

Vertical component of the anomalous field

Fig. 2(c) shows that the variations $Z_0(t)$ of the vertical component obtained at PDN station (with an Askania variograph) are very similar to the simultaneous variations of the horizontal differences $\Delta H_{i0}(t)$, $\Delta D_{i0}(t)$ between station FAN and station PDN. This observation holds for almost all the simultaneous recordings of Z, ΔH, ΔD we have collected (37 stations out of 40; in these stations in the vicinity of Perpignan, the characteristics of the anomalous field are different; these stations will not be considered in the present paper). Nevertheless, this similarity is not perfect, and does not hold for long periods. Indeed, ΔH, ΔD differences are, as we said, representative of the anomalous field; now, the vertical component $Z(t)$ has a normal part Z_n, generally small for periods from a few minutes to several hours (one order of

Downloaded from https://academic.oup.com/gji/article/1/4/583/570157 by U.S. Department of Justice user on 17 August 2022

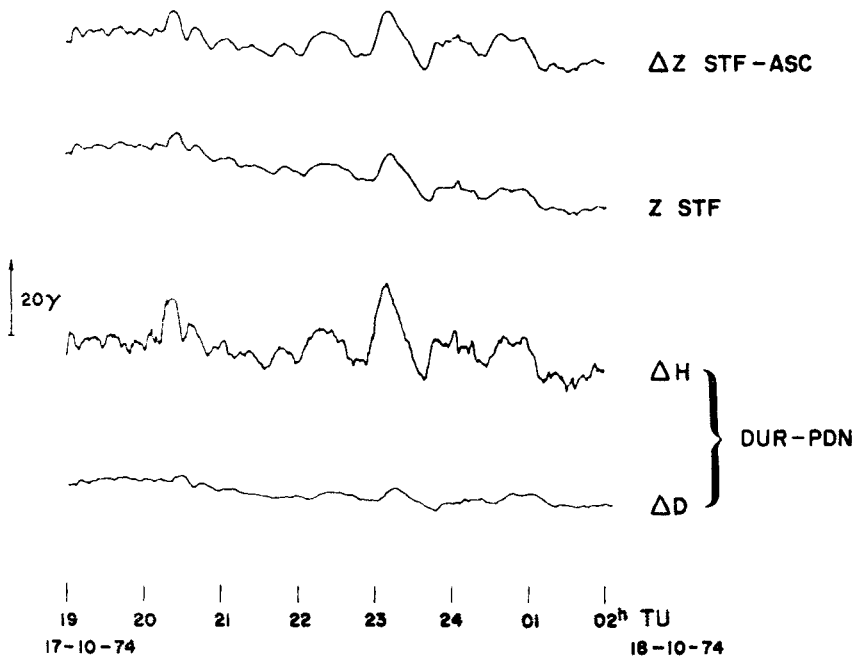

FIG. 4. Simultaneous variations of $\Delta H_{t0}(t)$, $\Delta D_{t0}(t)$, $Z_k(t)$, $\Delta Z_{k1}(t)$ on 1974 Oct. 17; S_t = DUR; S_k = STF; S_1 = ASC.

magnitude less than the normal horizontal variations), but not small for longer periods (daily variations for example). However, if the differences $\Delta Z_{ij}(t) = Z_i(t) - Z_j(t)$ between two stations S_i and S_j of the area concerned with the anomaly are computed, a close similarity of $\Delta Z(t)$ differences with $\Delta H(t)$ and $\Delta D(t)$ differences is found within the experimental errors. Such an example is illustrated by Fig. 4.

So we come to the conclusion that the anomalous field $\vec{B}_a(P, t)$ is *linearly polarized in space for periods from a few minutes to a few hours*; and, by generalizing formula (2), which was relative to the horizontal component only, we can write:

$$\vec{B}_a(P, t) = \vec{b}_a(P).R(t). \tag{3}$$

Contrary to what was done for the horizontal components obtained from the Mosnier variometers, the differences ΔZ were not systematically computed: first, because the Askania recordings do not lend themselves to such a treatment (the recording speed is low, and a good synchronization between different stations is difficult to obtain) second, because no Askania reference station was operated for the whole period of measurements (as was the case for PDN for Mosnier stations).

Normalization of the anomalous field

(a) *Horizontal component (Mosnier variographs).* Since it was not possible for us to have simultaneous recordings at all the stations of the three profiles $\alpha'\alpha$, $\beta'\beta$, $\gamma'\gamma$ (only six Mosnier stations were at our disposal), we had to resort to a normalizing

Downloaded from https://academic.oup.com/gji/article/14/583/570157 by U.S. Department of Justice user on 17 August 2022

process in order to be able to compare the anomalous field (defined on each profile by the differences Δ_{i0}) from one profile to another. For this purpose, two Mosnier variograph stations S_0(PDN), S_1(DUR) were operated during the whole experiment. The horizontal component of the anomalous field at the station S_i will be characterized by the following vector:

$$\vec{k}_H(S_i) \begin{cases} k_h(S_i) = \Delta H_{i0}(t)/\sqrt{(\Delta H_{10}^2(t)+\Delta D_{10}^2(t))} \\ k_d(S_i) = \Delta D_{i0}(t)/\sqrt{(\Delta H_{10}^2(t)+D_{10}^2(t))}. \end{cases}$$

This vector, which is independent of time, is, in the above mentioned conditions, proportional to the horizontal anomalous field $\vec{h}_a(S_i)$ defined in formula 2 which, anyhow, can be only defined up to a constant multiplicative factor. In practice, we have computed, for each station S_i, various values of $\vec{k}_H$ from several samples, each of them being about 10 hr long. The scattering of computed values $\vec{k}_H$ is less than 3° in azimuth and less than 3 per cent in modulus from one sample to another.

(b) *Vertical component (Askania variographs).* In all Askania stations (about 20 of them) which operated simultaneously with the Mosnier stations S_0 and S_1, it was possible to normalize the vertical component of the anomaly in the same way: at the Askania station S_j we define $k_Z(S_j) = Z_j(t)/\sqrt{(\Delta H_{10}^2(t)+\Delta D_{10}^2(t))}$. In doing so we consider Z and Z_a as identical, which is only an approximation as was said above; nevertheless, for Z variations with periods less than 1 or 2 hr this approximation is generally good (it would have been better to compute differences ΔZ_{i0}, ΔZ_{10}; we said above that it was difficult to compute systematically and accurately these differences). Of course, the accuracy of the determination of k_Z defined as previously is much poorer than that of $\vec{k}_H$.

Thus a vector $\vec{k}$ everywhere proportional to the anomaly vector $\vec{b}_a$ is obtained; it should be noticed that, according to the chosen station, what is known is either the vertical component k_Z (in an Askania station) or the horizontal component $\vec{k}_H$ (in a Mosnier station) of $\vec{k}$.

The recordings of the 16 other Askania stations could not be handled in the same way. They were dealt with in a less systematic fashion in the course of interpretation.

5. Geometry of the Northern Pyrenean anomaly

Fig. 5 gives the distribution of the elements of the vectors $\vec{k}$: $\vec{k}_H$ for Mosnier stations, k_Z for Askania stations. The curves of equal values of the modulus $|\vec{k}_H|$ have been drawn on the same figure and the line along which the Z component changes sign is also shown.

In order to obtain a more global and more illustrative representation of the $\vec{k}_H$ vector field, the observed values of $\vec{k}_H$ have been interpolated, taking into account the fact that $\vec{k}_H$ is the gradient of an harmonic potential ($\vec{k}_H = -\overrightarrow{\text{grad}}\, V$). In Fig. 6 lines of isovalues of the potential V as well as interpolated and observed $\vec{k}_H$ vectors have been drawn. This potential (V) has been calculated according to the method proposed by Gough & Reitzel (1969). In Fig. 6 lines of isovalues of the potential V (the zero level being arbitrary), as well as interpolated and observed $\vec{k}_H$ vectors are shown.

The direction of the vectors $\vec{k}_H$ is roughly NS in most of the studied area. However, in the West, an important change in the direction of the field of vectors from roughly NS to N 45° E occurs.

Although the iso$-k_H$ curves are oriented roughly SW–NE, the outline of the anomaly shows large deviations from two dimensionality. The anomaly is more spread in the West than in the East as is clearly shown in Fig. 7 which represents the modulus $|\vec{k}_H|$ plotted along the $\alpha'\alpha$, $\beta'\beta$, and $\gamma'\gamma$ profiles respectively. Notice also (Fig. 5) that the curve $Z = 0$ is not parallel to the line of maximum of k_H.

Downloaded from https://academic.oup.com/gji/article/14/583/570157 by U.S. Department of Justice user on 17 August 2022

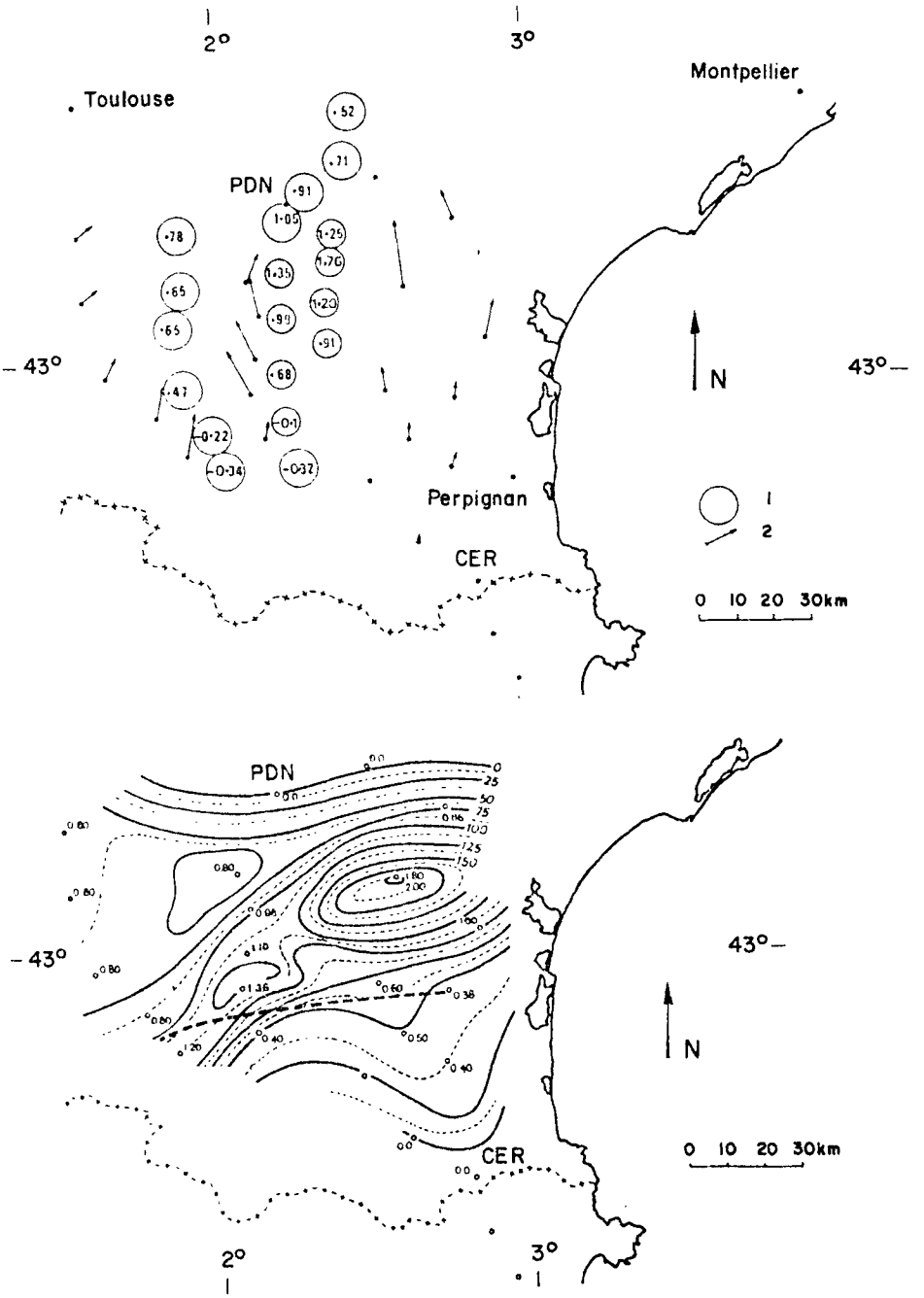

FIG. 5. Top: Observed values of $\vec{k}$. Arrows ($\vec{k}_H$) and numbers (k_Z) are measured in the same arbitrary units. (1): Values of k_z; (2): unit vector of $\vec{k}_H$. Bottom: Isovalue lines of $|\vec{k}_H|$. The line where $Z = 0$ is shown as a thick dotted line.

Downloaded from https://academic.oup.com/gji/article/1/4/583/570157 by U.S. Department of Justice user on 17 August 2022

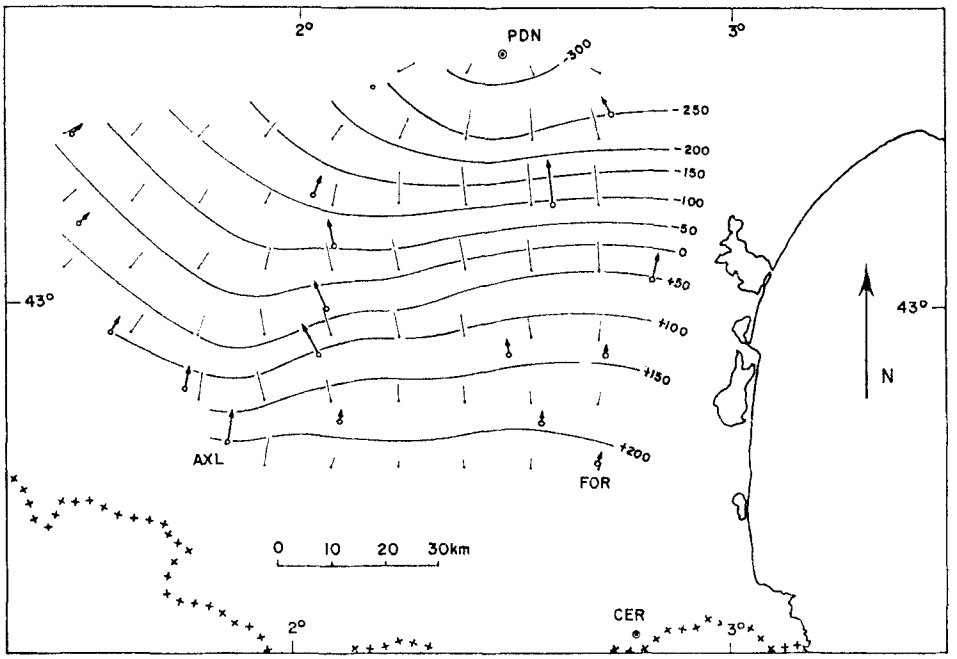

FIG. 6. Interpolated $\vec{k}_H$ (thin arrows), observed $\vec{k}_H$ (thick arrows) and magnetic equipotentials for V such that $\vec{k}_H = -\overrightarrow{\text{grad}}\, V$.

In order to check the consistency of $\vec{k}_H$ values with k_Z values, we compared the values of k_Z measured along profile B'B with k_Z' values calculated along profile $\beta'\beta$ from the values of k_H measured along this profile. This computation is made under the quite rough assumption of cylindricity. The values of k_Z' can be derived from k_H through a numerical integration (Schmucker 1970); here we have used for this calculation a formalism developed by Le Mouël, Courtillot & Galdeano (1974). The similarity in shape between the computed profile k_Z, and the observedp rofile k_Z is striking. However the k_Z' profile appears to be offset relatively to the k_Z profile by a quantity nearly constant along the whole profile. This offset can be partly a result of the departure of the true vector distribution from a two-dimensional one and partly due to the fact that the values of k_H outside the ranges of the profiles of measurement are unknown. It is also possible that, on the above described anomaly whose wavelength is typically 100 km, is superposed an anomaly with a much longer wavelength. The experimental values of k_Z (and k_H) would then be wrong by a nearly constant quantity along the profiles (and the CER station would then not be normal as far as this large wavelength anomaly is concerned).

6. Character of the currents responsible for the anomaly

We have shown that the anomalous field $\vec{B}_a(P, t)$ could be written in the form of a product of a space function by a time function:

$$\vec{B}_a(P, t) = \vec{b}_a(P).R\,(t) \tag{3}$$

for periods from a few minutes to a few hours. Such a separation of the variables implies that the electric currents responsible for the anomaly are not the result of local induction in a two-dimensional finite conductivity structure. Besides, the very large amplitude of the anomalous field (its horizontal component can be equal to the normal

Downloaded from https://academic.oup.com/gji/article/14/583/570157 by U.S. Department of Justice user on 17 August 2022

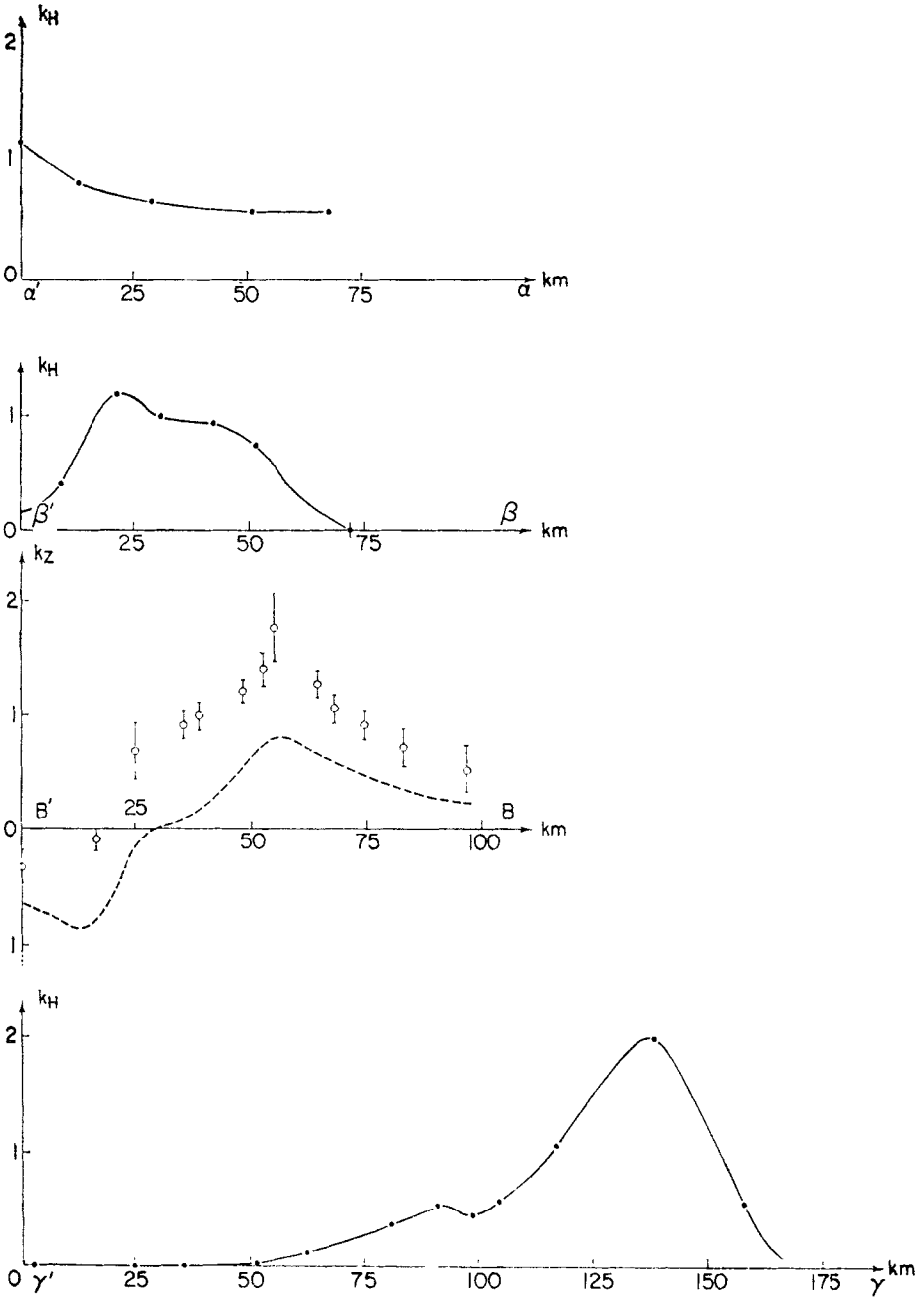

FIG. 7. From top to bottom: k_H profiles along $\alpha'\alpha$, $\beta'\beta$ and $\gamma'\gamma$ (*cf.* Fig. 1). Also shown is a k_Z profile along B'B (errors bars are plotted) together with a computed k_Z' profile deduced from k_H values along $\beta'\beta$ (dotted line).

Downloaded from https://academic.oup.com/gji/article/1/4/583/570157 by U.S. Department of Justice user on 17 August 2022

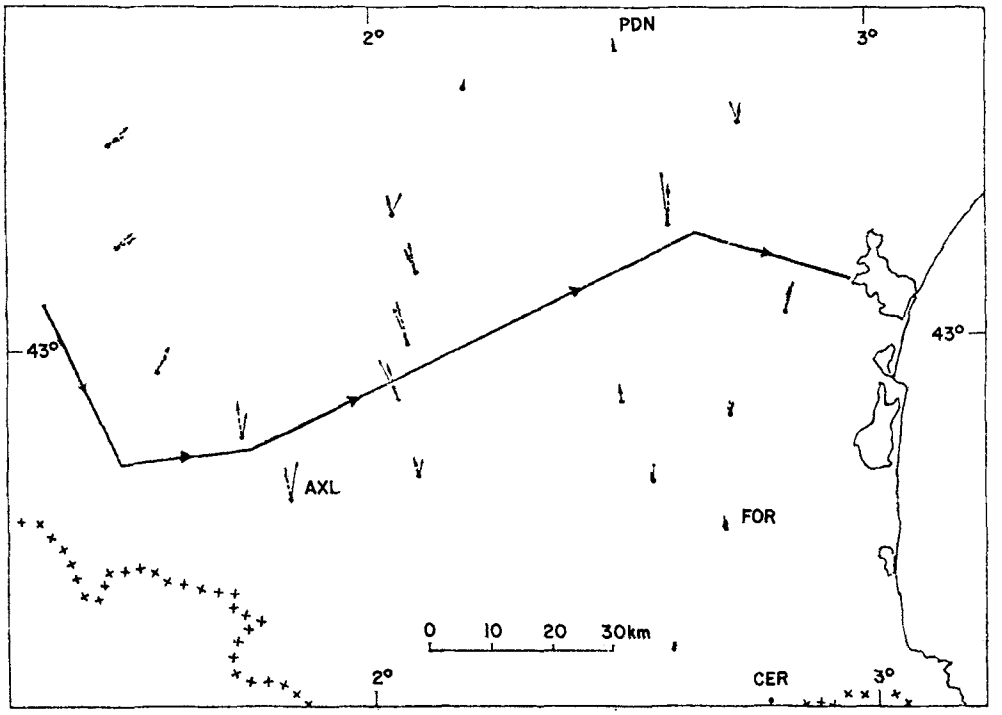

FIG. 8. Simplified model of equivalent currents—single broken line: equivalent current wire at a 17 km depth; observed $\vec{k}_H$ = continuous arrows, computed $\vec{k}_H$ = dashed arrows.

field) makes such an assumption as local induction in a cylindric body unrealistic, whatever the shape and the conductivity of this body may be . Thus, the anomaly we observe must be due to a current concentration (Porath, Gough & Campfield 1971). In fact, the simplest hypothesis—it is not of course the only one possible—that can be proposed concerning the currents responsible for the anomaly $\vec{B}_a(P, t)$ given by (3), is that these currents themselves can be separated in the following way:

$$\vec{I}_a(Q, t) = \vec{\imath}_a(Q).R\,(t) \tag{4}$$

Q being the current point of the substratum below the area concerned with the anomaly, $R(t)$ being the same function as in (3).

Contrary to what happens with direct local induction in a finite conductivity body, all the flux tubes of the current distribution (4) are in phase (besides we suppose that, at a given instant, the current flows in the same sense in all these current flux tubes). We will call such a current distribution a pseudo-direct one. Of course such currents cannot exist alone, they must be accompanied by return currents; but these return currents, whose paths are unknown, must lie outside the detection range of our instruments. The current concentration responsible for the observed anomaly $\vec{B}_a$ could be, for instance, a short circuit between currents flowing in the Mediterranean and in the bay of Biscay.

We have begun a study of the relationship between the temporal response function $R(t)$ and the normal field $\vec{B}_n(t)$. Our first results indicate a good correlation between $R(t)$ (or equivalently $\Delta H_{i0}(t)$, or $\Delta D_{i0}(t)$ ...) and the component of $\vec{B}_n(t)$ along a N50 °E direction. This study will be published later; in this paper we only deal with the geometry of the currents responsible for the anomaly, that is with function $\vec{\imath}_a(Q)$.

Downloaded from https://academic.oup.com/gji/article/14/583/570157 by U.S. Department of Justice user on 17 August 2022

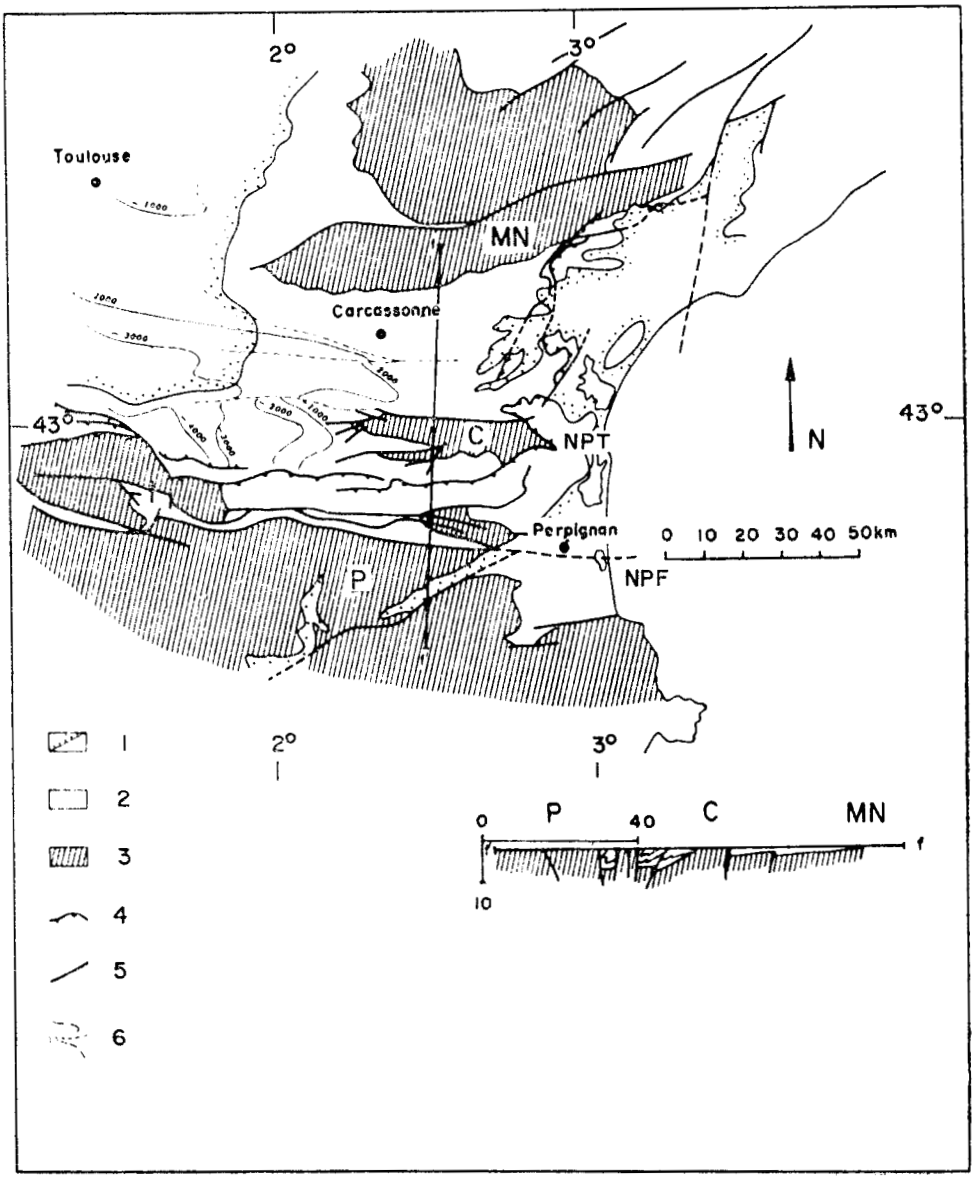

FIG. 9. Geological map of the studied region (after Choukroune & Séguret, 1973). (1) Oligocène and Post Oligocène, and (2) Mesozoic and eocene (Eocene Miocene basins); (3) Hercynian; (4) Overthrust; (5) Fault (6) Isobaths of the top of Hercynian basement in metres under the sea level. Bottom right: Geological cross-section along the f'f profile.

Depth of currents

It is well known that the determination of the currents $\vec{i}_a$ from the anomalous field $\vec{b}_a$ does not lead to a unique solution. At least, it is possible to estimate the maximum depth at which these currents can flow: it is the depth of a wire in which flows a current which creates an anomaly as similar as possible to the observed anomaly. The shape and depth of such a wire have been computed by using a non linear regression method (Fig. 8). (In this computation, we consider only the hori-

Downloaded from https://academic.oup.com/gji/article/1/4/583/570157 by U.S. Department of Justice user on 17 August 2022

zontal component $\vec{h}_a$ of $\vec{b}_a$ because it is more accurately defined than its vertical component z_a). The wire is 17 km deep.

7. Correlation with geological and additional geophysical data

We have estimated the maximum depth at which the currents could flow but not, of course, a minimum depth (except the surface). We will now summarize the local geology in the area we studied and will show that superficial sedimentary basins cannot account for the observed anomalous variations.

The structural map of the area (Fig. 9, after Choukroune & Séguret 1973) shows an overall E–W trend: this trend is inherited from paleozoic structures; these old structures, most of which have been reactived in more recent time, are from North to South: the Montagne Moire massif (MN), the Corbières massif (C) which is entirely surrounded by recent sedimentary basins and the Pyrenean chain sensu stricto (P). The fan-like tectonic setting of the whole area is clearly indicated by the small cross-section in Fig. 9. The surface expression of these accidents in the basement is materialized to the North of the Pyrenean chain by the North Pyrenean Frontal Thrust (NPT) and the North Pyrenean Fault (NPF). Over the paleozoic terrains are found tertiary sedimentary basins, with a thickness of sediments that can in places reach 3000 m and more. The northern basin (Carcassonne basin) is about 2000 m deep while the basin to the south of the Corbières massif has a pinched overthrust structure and is locally more than 5000 m deep. A fairly good correlation is found between the iso-k_H anomaly map (Fig. 5) and surface geology. The main focus of the anomaly (near CAP) seems at first sight to coincide with the trend and surface extension of the Carcassonne basin.

In order to see whether the geomagnetic anomaly could be explained by a superficial current flow in these basins, two kinds of electric measurements were undertaken. Electric sounding experiments first provided an estimate of the resistivity of the sediments: 30 Ωm. Telluric currents measurements then gave an estimate of the current density flowing in the sediments. Given the thickness and the conductivity of the sediments, the total contribution of these superficial currents to the anomaly could be estimated. In order to create an abnormal field $\vec{b}_a$ of about 10γ in intensity, the current density in the basins needs to be about 5 $\mu A/m^2$ (taking 3000 m for the mean depth of the basin), associated with an electric field of 150 mV km^{-1}. Now, in our experiments, values of the electric field associated with such values of the abnormal field $\vec{b}_a$ never exceeded 20 mV km^{-1} in the sedimentary basins. Thus, these basins can only account for 10–20 per cent of the observed effect and sources must exist at depths greater than 3–5 km and less than 15–20 km in depth. However, the superficial currents probably account for the short-wavelength irregularities which are observed in profiles from Fig. 7. The fact that there is a good correlation between surface geology and the anomaly in the eastern part of the studied area may be only due to the fact that both are separately governed by the overall palaeozoic trend which certainly extends to fairly large depths. In the West the correlation is not so good and the iso-k_H lines make a 45° angle with the E–W trend. This may be associated with an even deeper source (the intensity of the anomaly not being very large in the area) or with local tectonic complications (see Fig. 9).

Additional geophysical data may next be considered. As far as the gravity map of the area is concerned, the strong observed Bouguer anomalies are easily explained by the density contrasts which have been inferred from surface geology and petrography. In the same area, we have an aeromagnetic survey (Le Borgne & Le Mouël 1969); part of this survey is shown in Fig. 10 (anomalies at a 1000 m altitude computed by A. Galdeano). The correlation between this map and that of Fig. 5 is fairly convincing, in particular over the Carcassonne basin static magnetic anomaly ($\sim 50\gamma$).

Downloaded from https://academic.oup.com/gji/article/14/583/570157 by U.S. Department of Justice user on 17 August 2022

FIG. 10. Map of static magnetic field anomalies at 1000 m above sea level (from the aeromagnetic survey of France). Equidistance of curves is 10γ. The dotted lines represents the trend of the geomagnetic variation anomaly.

Finally, let us mention a seismic refraction profile at the longitude of the AA' profile (Bonnin 1968). This experiment pointed out a 10 km quasi-vertical upthrust of the Moho, approximately 20–30 km below the NPF (Fig. 9); these figures are only approximate, since the profile was not reversed.

One possible interpretation suggested by the geological observations summarized above is that the observed geomagnetic variations anomaly is due to currents flowing in very old sedimentary basins inside the paleozoic ' basement '. Such basin may have been considerably deformed (pinched) and possibly partly affected by metamorphism, but would retain electrical and magnetic properties different from those of the surrounding basement. The same rocks could be responsible for the observed magnetic anomalies. Such old intra-basement basins have indeed been found in the studied area in the course of oil-drilling, However it does not seem possible that these intra-basement basins are able to account for the bulk of the observed anomaly, whatever the thickness we can realistically assign to them.

A second interpretation is suggested by the upward deflection of the upper mantle as evidenced by the seismic profile. This deflection may be associated with a thermal anomaly and a similar deflection of isotherms. There is generally close correspondance of high conductivity with high temperature. Such a thermal origin for conductivity anomaly has often been invoked in the literature. However the wavelength of the observed geomagnetic variations anomaly appears to be too short to be linked with such a deflection of the isotherms. Furthermore, the conductivity contrasts due to this deflection does not seem to be sufficient to account for the observed anomaly.

Downloaded from https://academic.oup.com/gji/article/14/583/570157 by U.S. Department of Justice user on 17 August 2022

A third interpretation supported by the seismic data previously described is that the downwards extension of the major thrust faults and subvertical accidents such as the NP fault could be very deep and bring at some common depth different kinds of rocks, thus creating a lateral conductivity contrasts.

8. Conclusion

Our data do not allow us to give a truly quantative interpretation of the very large conductivity anomaly which we have described; we just pointed out a number of mechanisms that could be responsible for it and, at the same time, we pointed out correlations between various sources of data that cannot be ignored. The separation between the three mechanisms suggested above is a very artificial one, as all of them may occur in conjunction, all of them being genetically related to the tectonic setting of the whole area.

In conclusion, we would like to recall that, in the anomaly we have described, a *natural* separation of the space and time variables occurs. Local induction is not a likely mechanism to explain this anomaly and a strong current concentration is envisioned to take place.

Acknowledgments

This work was supported by Institut National d'Astronomie et de Géophysique through 'Action Thématique Programmée: Géodynamique de la Méditerranée occidentale et de ses abords'.

References

Bonnin, J., 1968. *Essai d'interprétation d'un profil seismique transversal aux Pyrénées*, USTL Montpellier, France; unpublished.

Choukroune, P. & Séguret, M., 1973. *Carte structurale des Pyrénées. U.S.T.L. Montpellier*, France; Elf. Erap.

Choukroune, P., Séguret, M. & Galdeano, A., 1973. Caractéristique et évolution structurale des Pyrénées: un modèle de relations entre zone orogénique et mouvement des plaques, *Bull. Soc. Géol. Fr.*, (7), **XV**, 600.

Gough, D. I. & Reitzel, J. S., 1969. Magnetic deep sounding and local conductivity anomalies, *The application of modern physics to the Earth and planetary interiors*, 139–153, ed. S. K. Runcorn, Interscience, New York.

Gough, D. I., 1973. The interpretation of magnetometer array studies, *Geophys. J. R. astr. Soc.*, **35**, 83–98.

Le Borgne, E. & Le Mouël, J. L., 1969. La réduction des observations et la précision des levés aéromagnétiques de la France continentale et de la Méditerranée occidentale, *Ann. Géophys.*, **25**, 371–379.

Le Mouël, J. L., Courtillot, V. & Galdeano, A., 1974. A simple formalism for the study of transformed aeromagnetic profiles, *J. geophys. Res.*, **79**, 324–331.

Mosnier, J., 1970. Variomètre sensible pour l'étude de la déclinaison. Etude théorique, *Ann. Géophys.*, **26**, 127–139.

Mosnier, J. & Yvetot, P., 1972. Nouveau type de variomètre à aimant asservi en direction, *Ann. Geophys.*, **28**, 219–224.

Porath, H., Gough, D. I. & Campfield, P. A., 1971. Conductive structures in the North Western United States and South West Canada, *Geophys. J. R. astr. Soc.*, **28**, 387–389.

Rikitake, T., 1966. *Electromagnetism and the Earth's interior*, Elsevier, Amsterdam, 308 pp.

Schmucker, U., 1970. Anomalies of geomagnetic variations in the South Western United States, *Bull. Scripps. Inst. Oceanography*, **13**, 1–165

Downloaded from https://academic.oup.com/gji/article/1/4/583/570157 by U.S. Department of Justice user on 17 August 2022